Electronic Supplementary Material (ESI) for Dalton Transactions.
This journal is © The Royal Society of Chemistry 2015

Supporting Information

A Family of Tetranuclear Quinolinolate Dy(III)-based Single-Molecule Magnets: Effects of Periphery Ligand Replacement on Their Magnetic Relaxation

Da Zhang,[a] Yong-Mei Tian,[a] Wen-Bin Sun,[a,*] Hong-Feng Li,[a] Peng Chen,[a] Yi-Quan Zhang,[b,*] and Peng-Fei Yan,[a,*]

[a.] Key Laboratory of Functional Inorganic Material Chemistry Ministry of Education, Heilongjiang University No.74, Xuefu Road Nangang District Harbin 150080, China.

[b.] Jiangsu Key Laboratory for NSLSCS, School of Physical Science and Technology, Nanjing Normal University, Nanjing 210023, China.

E-Mail: wenbinsun@126.com and zhangyiquan@njnu.edu.cn

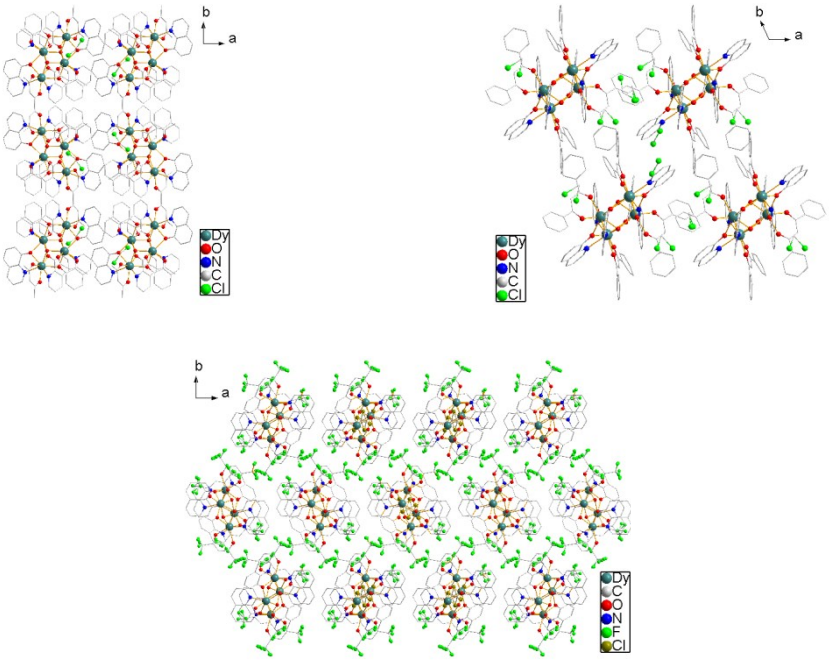

Fig. S1 Crystal packing of complexes **1** (top left), **2** (top right) and **3** (bottom) along c axis

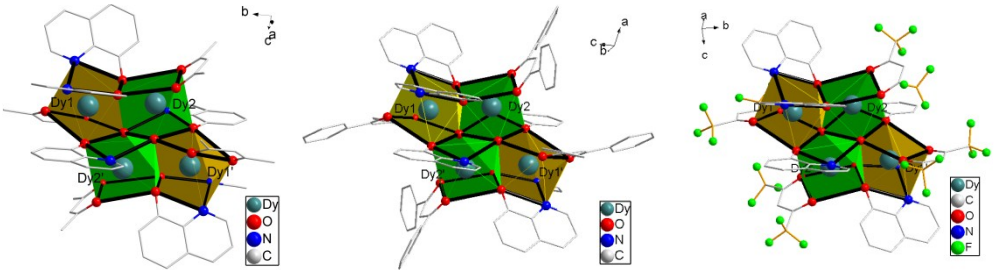

Fig. S2 Local coordination geometry of Dy^{3+} ions of complexes **1** (left), **2** (middle) and **3** (right).

Table S1. Dy^{III} geometry analysis of complexes **1**−**3** by SHAPE 2.1 software.

DyIII		Square antiprism (D4d)	Triangular dodecahedron (D2d)	Biaugmented trigonal prism (C2v)	Biaugmented trigonal prism J50 (C2v)
DyIII (**1**)	Dy1	0.968	2.101	1.545	2.126
	Dy2	1.515	1,425	2.371	3.048
DyIII (**2**)	Dy1	0.900	2.351	1.788	2.263
	Dy2	1.111	2.192	2.088	2.783
DyIII (**3**)	Dy1	0.668	2.403	1.788	2.529
	Dy2	0.936	2.061	2.315	3.069

Table S2 Selected bond lengths (Å) for complexes **1**−**3**.

1		2		3	
Dy(1)-O(7)	2.295(5)	Dy(1)-O(7)	2.290(4)	Dy(1)-O(8)	2.317(2)
Dy(1)-O(6)	2.320(5)	Dy(1)-O(6)	2.314(3)	Dy(1)-O(7)	2.345(2)
Dy(1)-O(8)′	2.326(5)	Dy(1)-O(8)′	2.355(3)	Dy(1)-O(3)	2.345(2)
Dy(1)-O(8)	2.347(5)	Dy(1)-O(2)′	2.359(4)	Dy(1)-O(2)	2.352(2)
Dy(1)-O(3)	2.360(4)	Dy(1)-O(8)	2.380(3)	Dy(1)-O(6)	2.366(2)
Dy(1)-O(2)	2.393(5)	Dy(1)-O(1)	2.404(4)	Dy(1)-O(8)′	2.367(2)
Dy(1)-O(1)	2.422(5)	Dy(1)-O(3)	2.409(4)	Dy(1)-O(1)′	2.384(2)
Dy(1)-N(3)	2.547(6)	Dy(1)-N(2)′	2.556(5)	Dy(1)-N(3)	2.503(3)
Dy(2)-O(4)	2.301(5)	Dy(2)-O(5)	2.319(4)	Dy(2)-O(8)	2.301(2)
Dy(2)-O(5)	2.314(5)	Dy(2)-O(4)	2.323(4)	Dy(2)-O(1)	2.316(2)
Dy(2)-O(8)	2.344(5)	Dy(2)-(8)O	2.331(3)	Dy(2)-O(5)	2.344(2)
Dy(2)-O(2)	2.361(5)	Dy(2)-O(1)	2.344(3)	Dy(2)-O(2)′	2.357(2)
Dy(2)-O(3)′	2.376(4)	Dy(2)-O(2)	2.366(4)	Dy(2)-O(3)	2.374(2)
Dy(2)-O(1)	2.381(5)	Dy(2)-O(3)	2.379(4)	Dy(2)-O(4)	2.387(2)
Dy(2)-N(2)	2.522(6)	Dy(2)-N(1)	2.538(5)	Dy(2)-N(1)	2.486(3)
Dy(2)-N(1)	2.556(6)	Dy(2)-N(3)	2.541(5)	Dy(2)-N(2)	2.523(3)

Table S3 Lengths (Å) for Dy1-Dy2 and Dy1-Dy2' of complexes **1**−**3**.

	1	2	3
Dy1-Dy2	3.5400(4)Å	3.5583(4)Å	3.4936(2)Å
Dy1-Dy2'	3.8449(5)Å	3.8531(4)Å	3.8172(4)Å

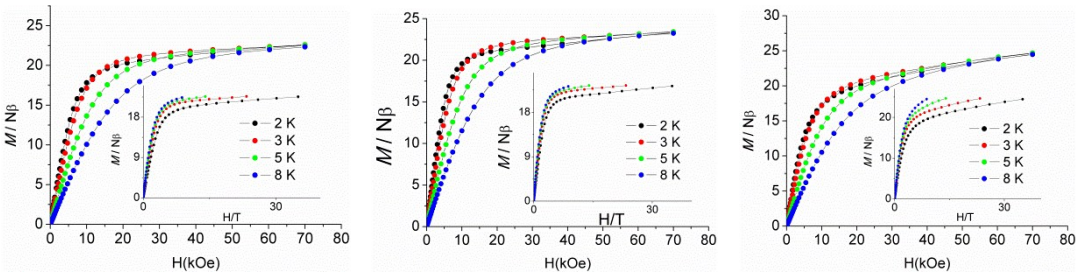

Fig. S3 Field dependences of magnetization in the field range 0−80 kOe and temperature range 2.0−8.0 K for complexes **1** (left), **2** (middle) and **3** (right). Inset: Plots of the reduced magnetization *M* versus *H*/*T*.

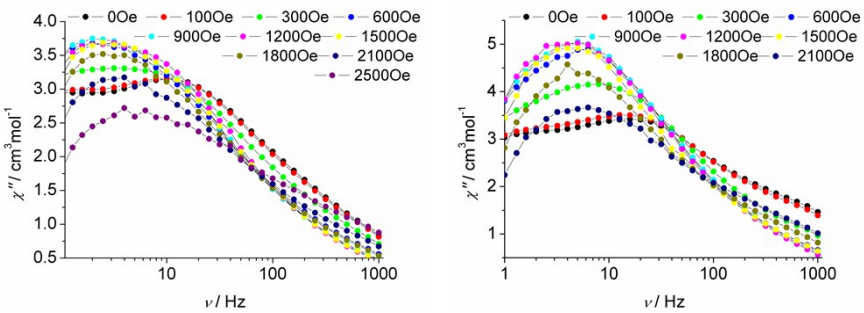

Fig. S4 Frequency dependence of the out-of-phase (χ″) ac susceptibility signals for **1** (left) between 0-2500 Oe, and **2** (right) between 0-2100 Oe.

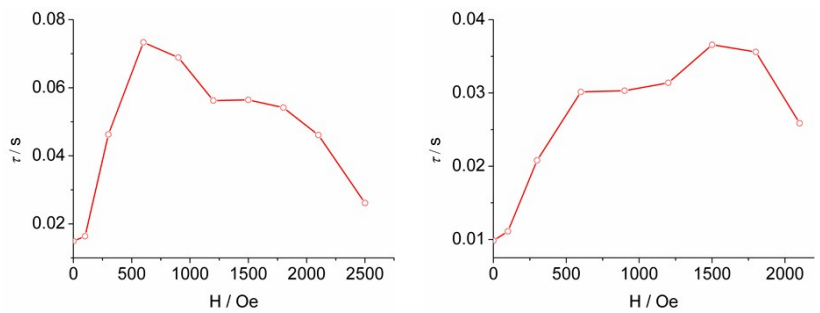

Fig. S5 Plots of the relaxation time τ versus H for **1** (left) between 0-2500 Oe, and **2** (right) between 0-2100 Oe.

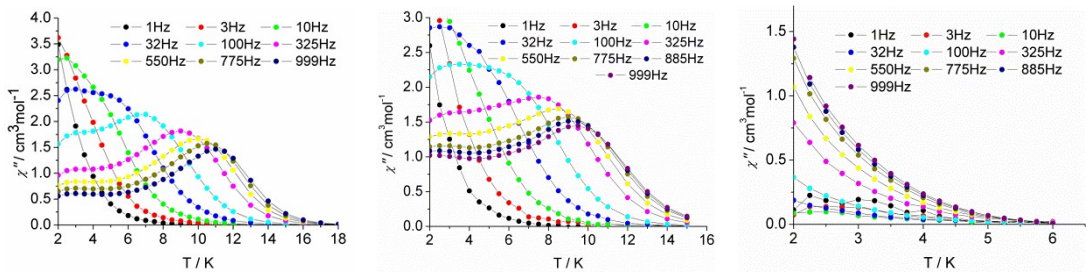

Fig. S6 Temperature dependence of the out-of-phase (χ″) ac susceptibility signals for **1** (left) under 600 Oe, and **2** (middle) and **3** (right) under 1500 Oe.

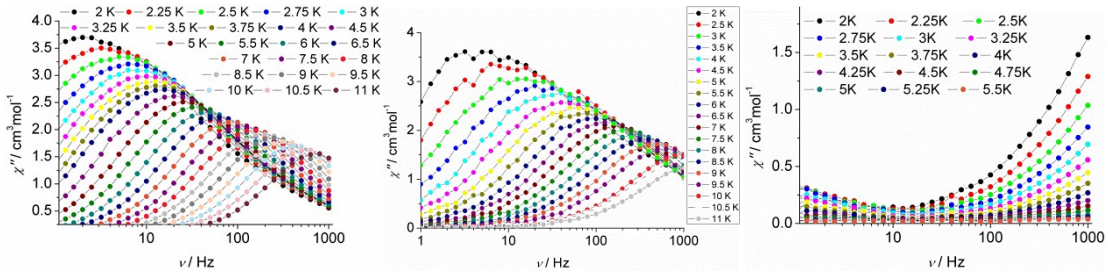

Fig. S7 Frequency dependence of the out-of-phase (χ″) ac susceptibility signals for **1** (left) under 600 Oe, and **2** (middle) and **3** (right) under 1500 Oe.

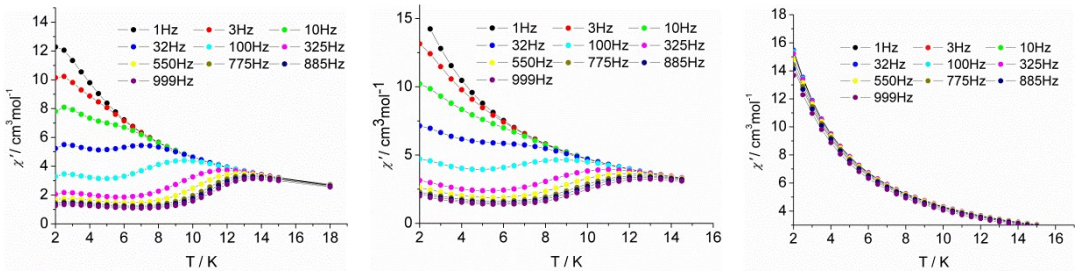

Fig. S8 Temperature dependence of the in-phase (χ') ac susceptibility signals for **1** (left), **2** (middle) and **3** (right) under zero-dc field.

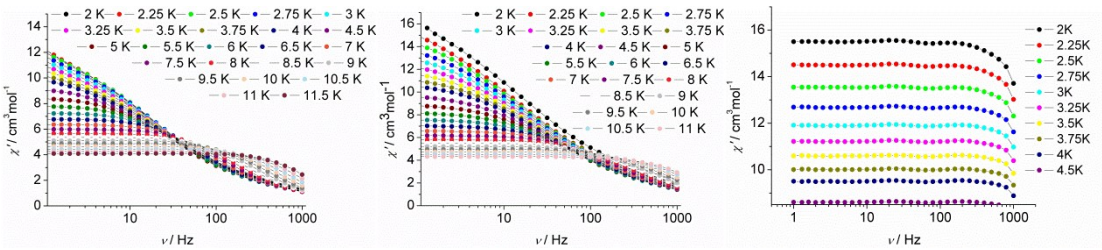

Fig. S9 Frequency dependence of the in-phase (χ') ac susceptibility signals for **1** (left), **2** (middle) and **3** (right) under zero-dc field.

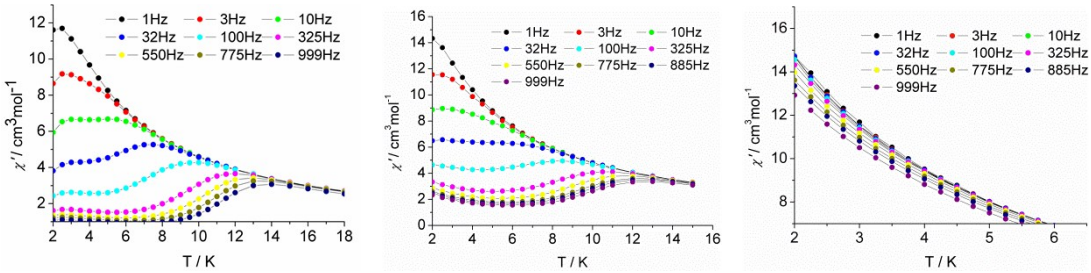

Fig. S10 Temperature dependence of the in-phase (χ') ac susceptibility signals for **1** (left) under 600 Oe, and **2** (middle) and **3** (right) under 1500 Oe.

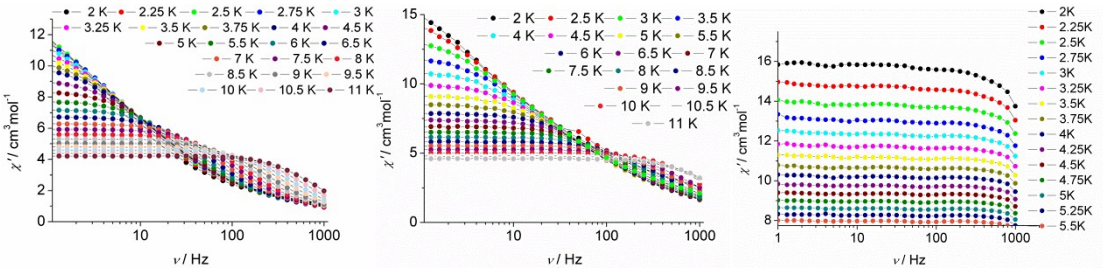

Fig. S11 Frequency dependence of the in-phase (χ') ac susceptibility signals for **1** (left) under 600 Oe, and **2** (middle) and **3** (right) under 1500 Oe.

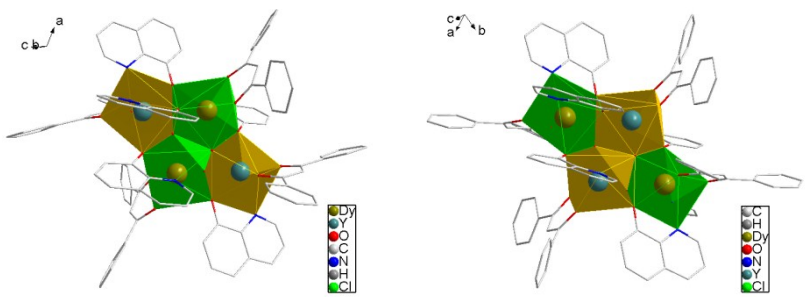

Fig. S12 Local coordination geometry of Dy^{3+} ions of complexes **2a** (left), **2b** (right).

Table S3 Crystal data and structures refinement for complexes **2a** and **2b**.

	2a	**2b**
Empirical formula	$C_{117}H_{86}Cl_6Dy_4N_6O_{16}$	$C_{120}H_{92}Cl_{12}Dy_4N_6O_{16}$
FW (g.mol-1)	2694.62	2949.40
Crystal system	triclinic	triclinic
Space group	P-1	P-1
T (K)	293(2)	293(2)
a (Å)	13.9257(11)	13.1075(4)
b (Å)	15.2084(12)	15.3796(6)
c (Å)	16.5342(10)	15.7951(6)
α (°)	110.987(7)	74.105(3)
β (°)	104.252(7)	87.634(3)
γ (°)	106.225(7)	77.013(3)
V (Å3)	2895.6(4)	2983.34(18)
ρcacd (Mg.m-3)	1.545	1.642
μ (mm-1)	2.753	2.809
F(000)	1324	1450
Collected reflections	26678	25835
Independent relections	13235	13607
Rint	0.0412	0.0284
R1 [I > 2σ(I)]	0.0822	0.0605
wR2 (all data)	0.2682	0.2122
GOF	1.072	1.035

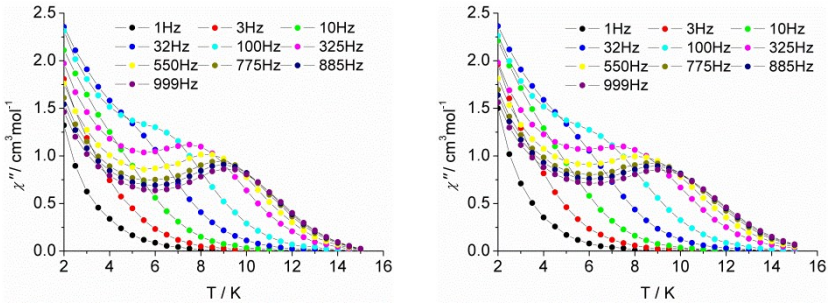

Fig. S13 Temperature dependence of the out-of-phase (χ″) ac susceptibility signals for complexes **2a** (left), **2b** (right) under 0 Oe.

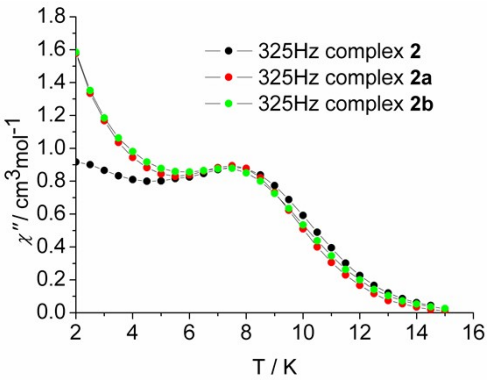

Fig. S14 Temperature dependence of the out-of-phase (χ″) ac susceptibility signals at 325Hz for complexes **2**, **2a**, **2b** under 0 Oe.

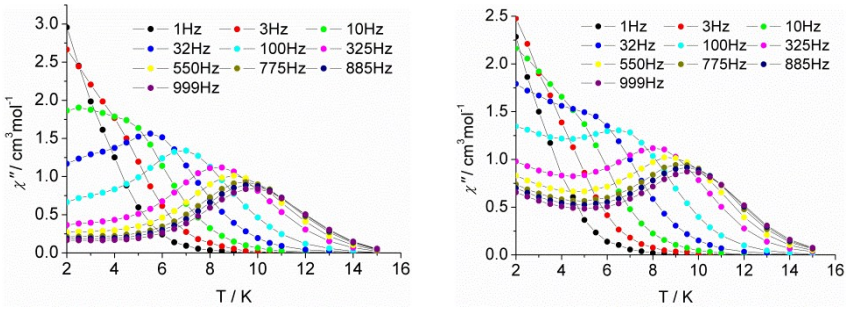

Fig. S15 Temperature dependence of the out-of-phase (χ″) ac susceptibility signals for complexes **2a** (left), **2b** (right) under 1500 Oe.

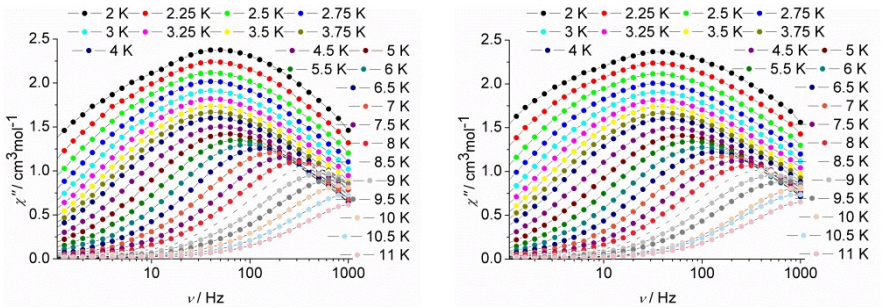

Fig. S16 Frequency dependence of the out-of-phase (χ″) ac susceptibility signals for **2a** (left), **2b** (right) under zero-dc field.

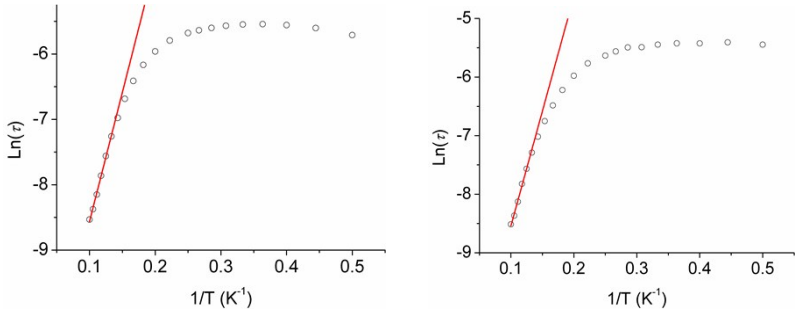

Fig. S17 Magnetization relaxation time, ln(τ) vs T^{-1} plot for complexes **2a** (left), **2b** (right) under zero dc field. The solid lines are fitted with the Arrhenius law (see text).

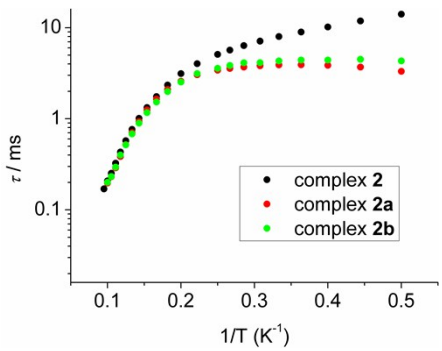

Fig. S18 Magnetization relaxation time, τ vs T^{-1} plot for complexes **2**, **2a**, **2b** under zero dc field.

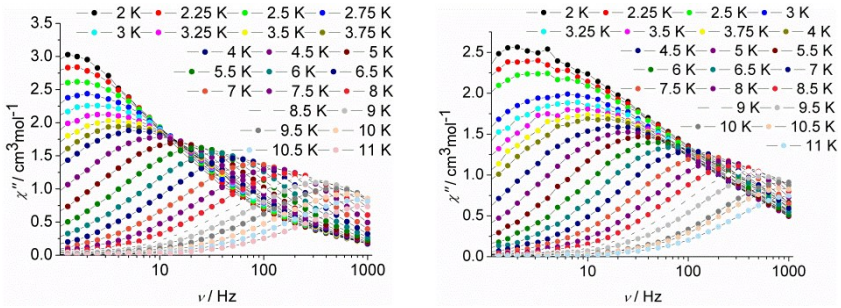

Fig. S19 Frequency dependence of the out-of-phase (χ″) ac susceptibility signals for **2a** (left), **2b** (right) under 1500 Oe.

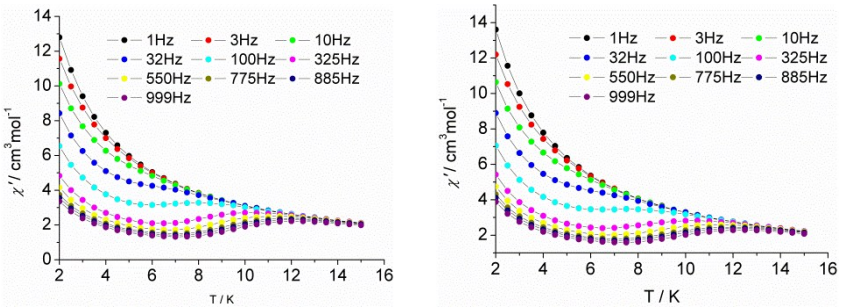

Fig. S20 Temperature dependence of the in-phase (χ') ac susceptibility signals for **2a** (left), **2b** (right) under zero-dc field.

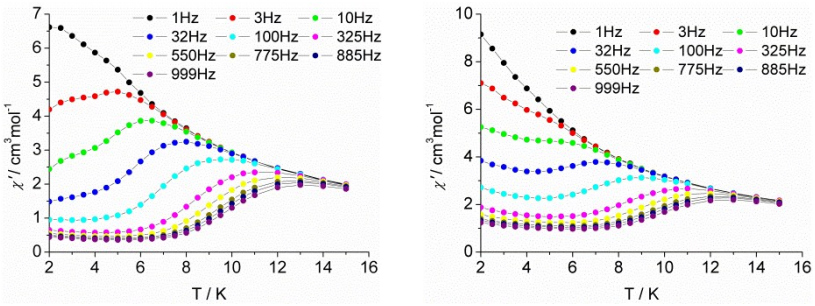

Fig. S21 Temperature dependence of the in-phase (χ') ac susceptibility signals for **2a** (left), **2b** (right) under 1500 Oe.

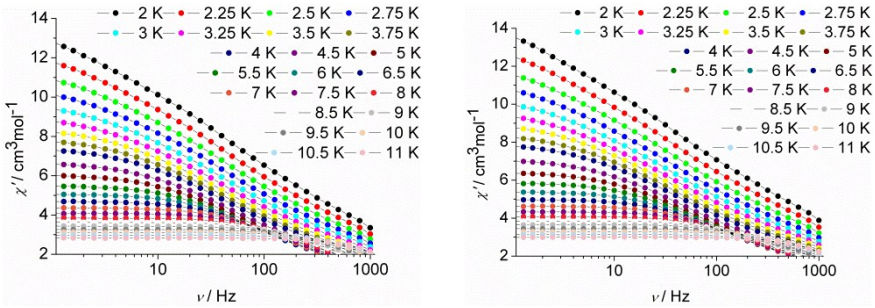

Fig. S22 Frequency dependence of the in-phase (χ') ac susceptibility signals for **2a** (left), **2b** (right) under zero-dc field.

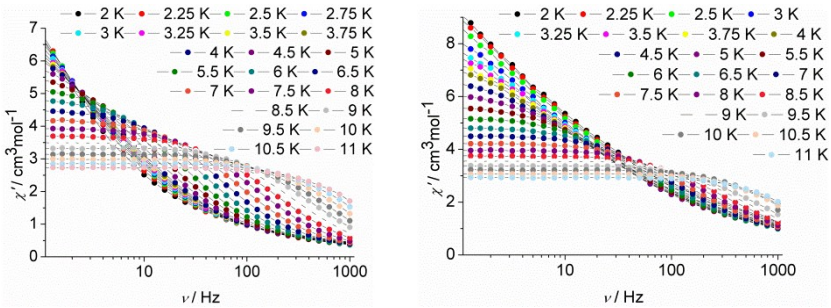

Fig. S23 Frequency dependence of the in-phase (χ') ac susceptibility signals for **2a** (left), **2b** (right) under 1500 Oe.

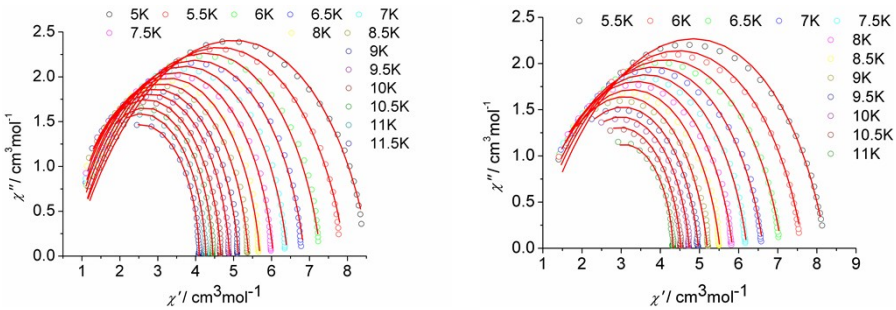

Fig. S24 Cole – Cole plots for temperatures between 5-11.5 K and 5.5-11 K for **1** (left) and **2** (right) under a zero dc field with the best fit to the generalized Debye model. The Solid lines represent fits to the data.

Table S4. Best fitted parameters (χ_T, χ_S, τ and α) with the extended Debye model for compound **1** at 0 Oe in the temperature range 2-11.5 K.

T/ K	χ_S / cm^3 mol^{-1}	χ_T / cm^3 mol^{-1}	τ/s	α
2	1.40000	12.69462	0.01372	0.30000
2.25	1.40063	12.65851	0.01226	0.30000
2.5	1.40135	12.40050	0.01115	0.29999
2.75	1.29987	11.90044	0.00977	0.29996
3	1.27154	11.48633	0.00913	0.29999
3.25	1.21885	11.06112	0.00846	0.29994
3.5	1.16010	10.65775	0.00787	0.29999
3.75	1.09814	10.27015	0.00730	0.29999
4	1.04558	9.91754	0.00677	0.30000
4.5	0.89965	9.23937	0.00559	0.29995
5	0.73919	8.59004	0.00441	0.29956
5.5	0.71865	7.94596	0.00343	0.27156
6	0.76134	7.29982	0.00260	0.22894
6.5	0.69682	6.86858	0.00202	0.21542
7	0.67177	6.42234	0.00154	0.19164
7.5	0.66784	6.04582	0.00120	0.17127
8	0.64708	5.69489	0.00092	0.15113
8.5	0.63117	5.39433	0.00072	0.13513
9	0.60953	5.12752	0.00056	0.12170
9.5	0.63827	4.89181	0.00043	0.10303
10	0.64663	4.66040	0.00034	0.08849
10.5	0.84869	4.45335	0.00028	0.05425
11	0.82531	4.26662	0.00021	0.05065
11.5	1.02308	4.09383	0.00017	0.02824

Table S5. Best fitted parameters (χ_T, χ_S, τ and α) with the extended Debye model for compound **2** at 0 Oe in the temperature range 2-11 K.

T/ K	χ_S / cm^3 mol^{-1}	χ_T / cm^3 mol^{-1}	τ/s	α
2	2.10000	15.69991	0.00905	0.29995
2.25	2.10000	15.40000	0.01110	0.30000
2.5	2.04688	14.52113	0.00983	0.29999
2.75	1.79057	13.70000	0.00853	0.29999
3	1.70000	12.97550	0.00772	0.30000
3.25	1.55640	12.28007	0.00690	0.29998
3.5	1.45872	11.70002	0.00630	0.30000
3.75	1.29997	11.07467	0.00553	0.29999
4	1.24819	10.56542	0.00504	0.30000
4.5	1.08302	9.65803	0.00404	0.29993
5	0.93481	8.90022	0.00321	0.29995
5.5	0.82947	8.23285	0.00251	0.29999
6	0.71719	7.64899	0.00192	0.29578
6.5	0.67001	7.10094	0.00146	0.27989
7	0.58196	6.63144	0.00108	0.26735
7.5	0.64247	6.21632	0.00083	0.24448
8	0.59264	5.84618	0.00062	0.23300
8.5	0.69731	5.52079	0.00048	0.21203
9	0.69998	5.19996	0.00035	0.19728
9.5	0.90060	4.97317	0.00028	0.18001
10	1.07914	4.73938	0.00023	0.15816
10.5	1.30000	4.52444	0.00018	0.13190
11	1.81836	4.32424	0.00018	0.06875

Computational details

There are two types of Dy^{3+} ions for each of complexes **1**–**3**, and thus we need to calculate two Dy^{3+} fragments for each of them. Complete-active-space self-consistent field (CASSCF) calculations on individual lanthanide Dy^{3+} fragment of the model structure (see Fig. S1) extracted from each complex on the basis of X-ray determined geometry have been carried out with MOLCAS 7.8 program package.[S1]

During the calculations, the other three Dy^{3+} ions for each complex were replaced by diamagnetic Lu^{3+}. The basis sets for all atoms are atomic natural orbitals from the MOLCAS ANO-RCC library: ANO-RCC-VTZP for Dy^{3+} ions; VTZ for close O and N; VDZ for distant atoms. The calculations employed the second order Douglas-Kroll-Hess Hamiltonian, where scalar relativistic contractions were taken into account in the basis set and the spin-orbit couplings were handled separately in the restricted

active space state interaction (RASSI-SO) procedure. For the fragment of Dy^{3+}, active electrons in 7 active spaces include all *f* electrons (CAS(9 in 7) in the CASSCF calculation. We have mixed the maximum number of spin-free state which was possible with our hardware (all from 21 sextets, 128 from 224 quadruplets, 130 from 490 doublets for the Dy^{3+} fragment).

To fit the exchange interactions in four complexes, we took two steps to obtain them. Firstly, we calculated one Dy^{3+} fragment using CASSCF to obtain the corresponding magnetic properties. And then, the exchange interaction between the magnetic centers is considered within the Lines model,[S2] while the account of the dipole-dipole magnetic coupling is treated exactly. The Lines model is effective and has been successfully used widely in the research field of f-element single-molecule magnets.[S3]

For each of complexes **1**–**3**, there are three types of *J* (see Fig. S1).

The exchange Hamiltonian is:

$$\hat{H}_{exch} = -J_1^{total}\,\hat{\tilde{S}}_{Dy1}\,\hat{\tilde{S}}_{Dy2} - J_2^{total}\,\hat{\tilde{S}}_{Dy3}\,\hat{\tilde{S}}_{Dy4} - J_3^{total}(\hat{\tilde{S}}_{Dy1}\,\hat{\tilde{S}}_{Dy3} + \hat{\tilde{S}}_{Dy1}\,\hat{\tilde{S}}_{Dy4} + \hat{\tilde{S}}_{Dy2}\,\hat{\tilde{S}}_{Dy3} + \tilde{S}_{Dy2}\,\hat{\tilde{S}}_{Dy4}) \qquad \text{(S1)}$$

The J_1^{total}, J_2^{total} and J_3^{total} are the parameters of the total magnetic interaction ($J^{total} = J^{diploar} + J^{exchange}$) between magnetic center ions. The $\hat{\tilde{S}}_{Dy}$ = ±1/2 are the ground pseudospin on the Dy^{3+} sites. The dipolar magnetic coupling can be calculated exactly, while the exchange coupling constants were fitted through comparison of the computed and measured magnetic susceptibility and molar magnetization using the POLY_ANISO program.[S4]

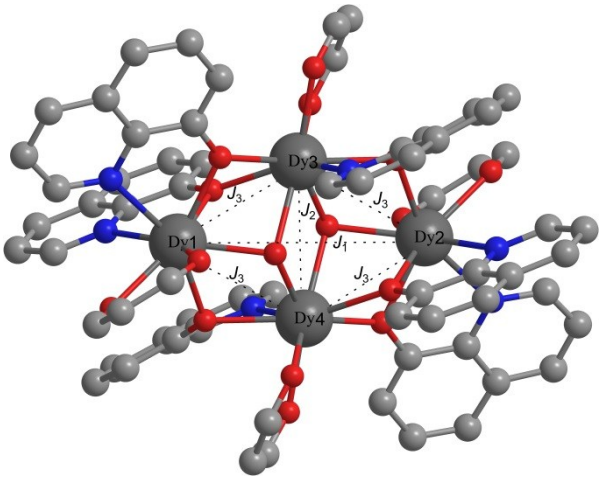

Fig. S25 Three types of J_1, J_2 and J_3 in complex **1.**

Table S6. Energies (cm^{-1}) and ***g*** (g_x, g_y, g_z) tensors of the lowest spin-orbit states on two types of Dy^{3+} fragments (see Fig. S23) for each of **1**–**3**.

1				**2**			
Dy1(Dy2)		Dy3(Dy4)		Dy1(Dy2)		Dy3(Dy4)	
E	*g*	*E*	*g*	*E*	*g*	*E*	*g*
0.00	0.006 0.008 19.697	0.00	0.016 0.026 19.524	0.00	0.011 0.015 19.680	0.00	0.110 0.205 19.236
116.81	0.297 0.340 16.982	132.54	0.137 0.262 16.168	120.59	0.374 0.574 16.713	73.66	1.154 3.303 9.784
204.49	2.057 3.107 12.554	205.51	2.157 3.195 11.931	197.41	1.682 2.662 13.125	83.69	0.246 3.721 8.946
251.99	1.073 5.115 12.020	238.21	0.078 3.993 9.567	242.88	1.003 3.267 9.848	118.49	8.899 5.630 0.275
304.78	8.709 4.910 0.643	278.20	7.939 5.043 0.598	305.55	2.794 4.954 9.332	142.49	3.733 4.941 12.490
350.41	3.097 3.851 12.531	302.91	1.709 5.390 14.032	351.48	2.2773 5.086 12.860	159.89	0.452 1.515 15.051
382.63	0.681 1.527 17.997	410.15	0.050 0.110 18.297	436.26	0.177 0.327 18.333	231.89	0.198 0.243 18.761
549.53	0.008 0.017 19.777	505.32	0.016 0.038 19.285	606.31	0.038 0.087 19.644	482.09	0.002 0.003 19.788

3			
Dy1(Dy2)		Dy3(Dy4)	
E	*g*	*E*	*g*
0.00	0.025 0.039 19.470	0.00	0.075 0.162 19.307
107.22	0.695 1.162 15.671	83.62	1.886 5.407 12.737
167.14	1.905 2.842 12.981	112.49	8.036 4.850 1.145
217.33	0.207 3.983 10.974	151.14	2.223 6.329 10.592
267.85	9.829 5.443 0.658	194.94	1.322 2.035 12.141
292.58	2.199 4.104 13.936	252.85	0.088 0.104 17.175
322.94	0.365 1.043 17.866	367.19	0.024 0.034 18.315
487.86	0.009 0.026 19.723	512.11	0.005 0.011 19.441

Table S7. Fitted exchange coupling constants J_{exch} and the calculated dipole-dipole interactions $J_{dipolar}$ between Dy^{3+} ions in **1**–**3** (cm^{-1}).

		J_1	J_2	J_3
1	$J_{dipolar}$	0.11	4.7	0.34
	J_{exch}	0.25	–1.0	–1.9
	J	0.36	3.7	–1.56
2	$J_{dipolar}$	0.20	3.9	0.33
	J_{exch}	0.75	5.5	–1.53
	J	0.95	9.4	–1.20
3	$J_{dipolar}$	0.10	2.1	–2.9
	J_{exch}	1.0	3.5	–1.13
	J	1.1	5.6	–4.03

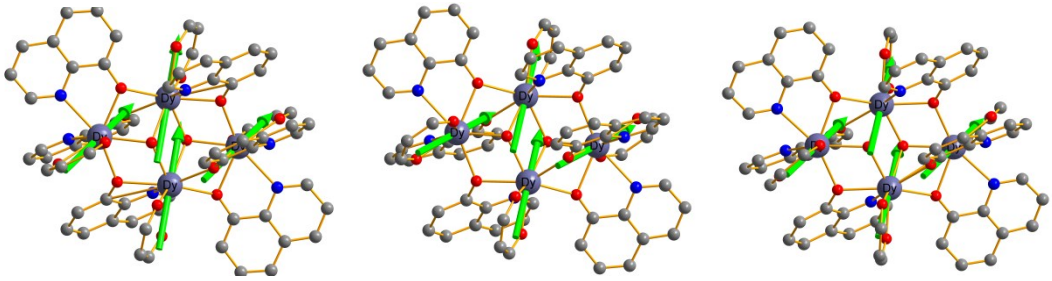

Fig. S26 Orientations of the local main magnetic axes of the ground doublets on Dy^{III} ions of **1** (left), **2** (middle) and **3** (right).

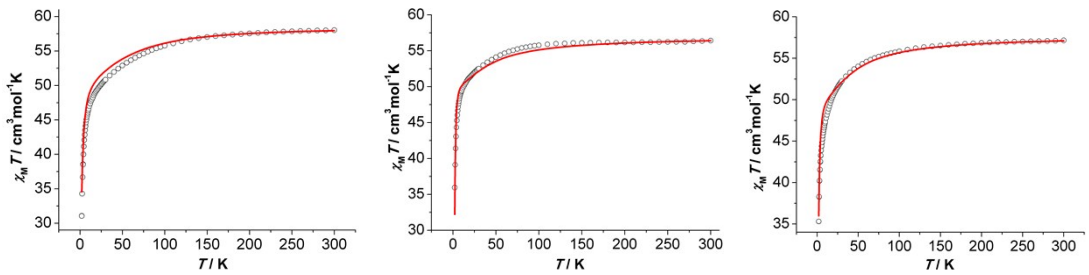

Fig. S27 Calculated (red solid line) and experimental data of magnetic susceptibility of **1** (left), **2** (middle) and **3** (right).

The intermolecular interactions zJ' of **1**–**3** were set to 0 cm^{-1}.

Table S8. Angles (°) and Distance on Dy1 and Dy2.

	Angles (°) between two easy axis	Angles (°) between easy axis on Dy1 and Dy1-Dy2	Angles (°) between easy axis on Dy2 and Dy1-Dy2	Angles (°) between easy axis and local symmetry axis on Dy1	Angles (°) between easy axis and local symmetry axis on Dy2
1	40.6	49.6	35.7	52.819	42.884
2	40.0	48.8	35.8	54.281	45.325
3	25.0	46.6	38.4	56.817	43.901

References:

S1 G. Karlström, R. Lindh, P.-Å. Malmqvist, B. O. Roos, U. Ryde, V. Veryazov, P.-O. Widmark, M. Cossi, B. Schimmelpfennig, P. Neograd y, L. Seijo, MOLCAS: a Program Package for Computational Chemistry. *Comput. Mater. Sci.*, 2003, **28**, 222.

S2 M. E. Lines, *J. Chem. Phys*., 1971, **55,** 2977.

S3 (a) K. C. Mondal, A. Sundt, Y. H. Lan, G. E. Kostakis, O. Waldmann, L. Ungur, L. F. Chibotaru, C. E. Anson, A. K. Powell, *Angew. Chem. Int. Ed*., 2012, **51**, 7550; (b) S. K. Langley, D. P. Wielechowski, V. Vieru, N. F. Chilton, B. Moubaraki, B. F. Abrahams, L. F. Chibotaru, K. S. Murray, *Angew. Chem. Int. Ed*., 2013, **52**, 12014.

S4 (a) L. F. Chibotaru, L. Ungur, A. Soncini, *Angew. Chem. Int. Ed.*, 2008, **47**, 4126; (b) L. Ungur, W. Van denHeuvel, L. F. Chibotaru, *New J. Chem.*, 2009, 33, 1224; (c) L. F. Chibotaru, L. Ungur, C. Aronica, H. Elmoll, G. Pilet, D. Luneau, D. *J. Am. Chem. Soc.*, 2008, **130**, 12445.